PREPARATION OF GRAPHENE OXIDE REINFORCED POLY (METHYL METHACRYLATE)

S. Morimune[1], T. Nishino[1]* and T. Goto[2]

[1]*Department of Chemical Science and Engineering, Kobe University, Rokko, Nada, Kobe, Japan*
[2]*Mitsubishi Gas Chem. Inc., Niijyuku, Katsushika, Tokyo,Japan*
**tnishino@kobe-u.ac.jp*

Keywords: Graphene oxide, Poly (methyl methacrylate), Mechanical Properties, Thermal Properties, Barrier Properties.

Abstract
In recent years, graphene oxide (GO) has been often used as a filler for the polymer nanocomposites because of their excellent properties. Previously, some groups conducted on poly (methyl methacrylate) (PMMA)/GO nanocomposites, which were prepared using organic solutions and/or surfactants. To provide an alternative to conventional procedures for fabricating, we have developed an environmentally friendly technique in which PMMA is polymerized by soap-free emulsion polymerization and incorporated with GO using water as a processing medium. Experimental results showed that the fabricated PMMA/GO nanocomposites had excellent mechanical, thermal, and O_2 barrier properties with the nano-dispersion of GO.

1 Introduction
Graphene, which consists of a single sheet of graphite, has been one of the most in-demand materials of the past decade. An enormous amount of research on graphene has been conducted and its excellent mechanical, thermal, and electrical properties have been revealed. Graphene is clearly one of the most promising materials for developments in nanotechnology across many fields because of its´ Young's modulus of 1 TPa, ultimate strength of 130 GPa, and the thermal conductivity of 5000 W/mK. [1,2] Graphene oxide (GO), which is the intermediate during the chemical processing of graphene, bears oxygen-containing functional groups on the basal planes and edges of graphene. These groups attach the characteristics of aqueous solution processability to the pristine graphene.
Recently, carbon-based nanomaterials have often been used for the filler of polymer nanocomposites. [3-5] Among them, carbon nanotubes (CNTs) have been considered potential candidates for many applications in nanotechnology due to their very high aspect ratio and unique electrical, thermal, and mechanical properties. However, in polymer matrices, CNTs tend to bundle together and form macro/micro aggregates which can cause defects in the material. Many efforts have been made to improve the dispersibility of CNTs in polymer matrices: for example, by the surface modification of CNTs. [6-10] Contrary to CNTs, GO possesses aqueous solution processability, and nano-disperse in the polymer matrices by simple process. Therefore, GO can impart the excellent properties, that are characteristic of the all carbon-based nanomaterials, to the polymer nanocomposites. Moreover, the nano-dispersion of the anisotropic structure of GO, as well as clay, is expected to significantly

impart excellent reinforcement effects to nanocomposites materials because of its high aspect ratio and large surface area. Therefore, the development of GO/polymer nanocomposites has attracted a great deal of attentions among researchers all over the world.

So far, many groups have reported on GO reinforced polymer nanocomposites using hydrophilic polymer, such as poly (ethylene oxide) or poly (vinyl alcohol) (PVA). [11,12] We ourselves have revealed the excellent reinforcement effect of GO in PVA/GO nanocomposites. [13] Nanocomposites with GO have also been produced using hydrophobic polymer, including polystyrene (PS), polyurethane (PU), and poly (methyl methacrylate) (PMMA). [14] PMMA/GO nanocomposites have been prepared by several procedures. For example, dissolving PMMA using an organic solvent such as dimethylformamide mixed with GO powder under vigorous stirring. PMMA/GO suspension has been fabricated into films by the casting method, vacuum-assisted self-assembly, and the layer-by-layer method. [15,16] However, the organic solvents and surfactants used in these processes are harmful to the environment.

In this study, we propose a new, environmentally friendly process for the preparation of PMMA/GO nanocomposites. Instead of using the organic solvent/surfactant combination, we mixed PMMA from soap-free emulsion polymerization with GO aqueous suspension. This simple and environmentally friendly process enables the GO to be dispersed in the PMMA homogeneously. Furthermore, it is easy to control a wide range of GO content. We also found that the resultant PMMA/GO nanocomposites had excellent enhancements of their mechanical, thermal, and O_2 barrier properties.

2 Materials and testing methods

2.1 Materials

GO aqueous suspension with a content of 1 % w/w was supplied by Mitsubishi Gas Chemical Inc. GO was synthesized from graphite using the Hummers' method.[17] Methyl methacrylate monomer (MMA, Sigma Aldrich Co.) was distilled under nitrogen at reduced pressure. Potassium peroxydisulfate (KPS, Sigma Aldrich Co.), the initiator, was recrystallized and dried in vacuum. Hydrochloric acid (HCl, Sigma Aldrich Co.) was used as supplied.

2.2 Sample preparation

PMMA. First, we performed soap-free emulsion polymerization. Distilled water (300 g), MMA monomer (50 g), and KPS (0.5 % w/w vs. MMA) was sequentially added to the flask. The mixture was then stirred at 330 rpm at 70 °C for 12 h. The average diameter of the PMMA particle was observed as 450 ± 20 nm using a scanning electron microscope (SEM) (TSM-5610LVS, JEOL Ltd.) at an accelerating voltage of 10 kV. Pt/Pd was deposited on the sample surface prior to observation. The average molecular weight of the PMMA was 440,000 (the degree of polymerization = 4400), which was analyzed as solutions in chloroform of 0.5 % w/w by gel permeation chromatography (HITACHI L-7000 Series, Hitachi Ltd.). The flow rate was 1 ml/min with the temperature set to 10 °C.

PMMA/GO nanocomposites. GO aqueous suspension (1 % w/w) was added to the PMMA emulsion and stirred for 1 day. Subsequently, 1 % w/w HCl aqueous solution was added dropwise to the mixture while stirring. The co-aggregated precipitant of PMMA/GO was rinsed with distilled water and dried in the oven at 50 °C and then in vacuum at 40 °C. PMMA/GO powder was melt-pressed at 180 °C for 15 min under 6 MPa. The amount (0–10 % w/w vs. PMMA) of the GO content in the nanocomposite was adjusted by changing the amount of GO aqueous suspension added.

2.3 Characterization

Atomic force microscopic (AFM) analysis was performed on the GO with a Nano Navi Station/E-sweep (Seiko Instruments Inc.). A silicon cantilever probe was used in the tapping mode in air. The GO aqueous suspension was diluted with distilled water and spin-coated on a

silicon wafer. The Fourier transferred infrared (FTIR) spectrometery (Spectrum GX FT-IR System I-KS, Perkin Elmer) was performed at a resolution of 2 cm^{-1}. The accumulated number of scans was 10. X-ray photoelectron spectroscopy (XPS) measurements were conducted for the GO powder on an indium ingot using an ESCA-850 spectrometer (Shimadzu Co.) equipped with MgKα radiation generated at 8 kV and 30 mA. X-ray diffraction was carried out with an X-ray diffractometer (RINT2100, Rigaku). The specimens were irradiated with a Ni-filtered CuKα radiation beam operated at 40 kV and 20 mA. The scanning speed was 1.0 degree/min, and the $2\theta/\theta$ scan data were collected at 0.02 degree intervals.

The tensile test was conducted using an Autograph AGS-1kND (Shimadzu Co.) with a cross head speed of 2 mm/min. More than ten specimens were tested with the initial length of 20 mm. The toughness (K), equal to the area surrounded by the stress (σ)–strain (ε) curve, was calculated as

$$K = \int_{\varepsilon=0}^{\varepsilon=\varepsilon_{\max}} \sigma \cdot \mathrm{d}\varepsilon / \rho \,(\mathrm{J/g}), \tag{1}$$

where σ is the stress (Pa), ε is the strain, and ρ is the density (g/m^3). Dynamic mechanical analyses (DMAs) were carried out using a dynamic mechanical analyzer (DVA-220S, ITK Co., Ltd.). A heating rate of 6 °C/min and a frequency of 10 Hz were set under nitrogen flow.

Differential scanning calorimetry (DSC) was performed with a differential scanning calorimeter (DSC-220CU, Seiko Instruments Inc.) under nitrogen flow at a heating rate of 10 °C/min. The thermal decomposition temperature (T_d) was measured by a thermogravimeter (TG) (TG/DTA-220CU, Seiko Instruments Inc.) at a heating rate of 10 °C/min under nitrogen flow. T_d was defined as a temperature of 5 % thermal weight loss. O_2 gas permeability was measured at 25 °C and relative humidity of 50 % on an OX-TRAN 2/21 (MOCON Inc.). The thickness of the specimens was 1 mm.

3. Results and Discussion

3.1 Characterization

Figure 1(a) shows the AFM image and the height profile of the GO along the line. The GO sheet had an irregular form, with some wrinkles and folding on the surface and edge. Judging from the height profile, the GO thickness was 0.8–1.0 nm with an average aspect ratio of 3000. It is apparent that the GO sheets are fully exfoliated and dispersed as monolayers in the aqueous suspension. The FTIR spectrum of GO is shown in Figure 1(b). The spectrum shows the characteristic absorption bands of GO. The band at 1622 cm^{-1} can be assigned to the stretching vibration of an aromatic sp^2 carbon bond. The bands at approximately 2915 cm^{-1} and 1352 cm^{-1} are attributed to aliphatic C–H stretching and deformation vibration, respectively. [18] In addition to the bands derived from the structure of graphene, which are planar sheets of sp^2-bonded carbon atoms, the oxygen-containing functional groups were also observed. The bands at 1733 cm^{-1}, 1225 cm^{-1} and 1075 cm^{-1} can be assigned as C=O stretching, C–OH bending and C–O stretching, respectively. [19] Furthermore, the band at 975 cm^{-1} can be assigned as the symmetrical epoxy ring deformation as well as the out-of-plane wagging of O–H–O. [20] The hydroxyl groups appeared at 3404 cm^{-1} (O–H stretching vibration) and 1622 cm^{-1} (O–H bending vibration), which included adsorbed water on the GO surface in air. [21,22] The XPS analysis revealed that GO contains 27.8 % oxygen, which can be related to the oxygen-containing groups as noted above. Judging from the results of FTIR and XPS, the surface of GO was oxidized adequately, which resulted in the nanodispersion of GO in an aqueous medium.

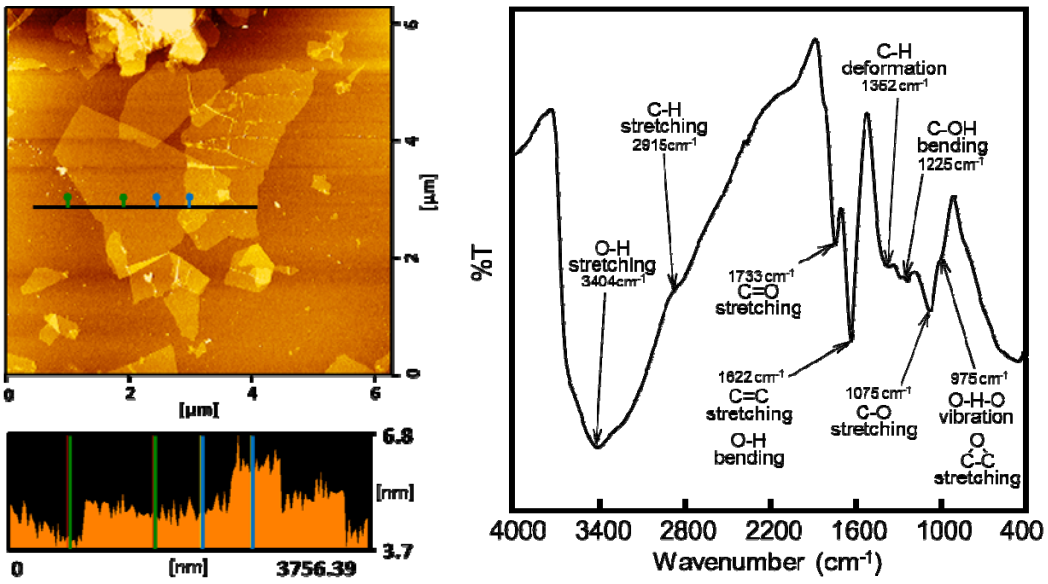

Figure 1. (a) AFM image and height profile of GO, (b) FT-IR spectrum of GO.

Figure 2 shows X-ray diffraction profiles of the PMMA, PMMA/GO nanocomposites, and GO. The GO was dried from the aqueous suspension. On the profile of GO, the characteristic peak of 001 reflection corresponding to the GO interlayer appeared clearly at $2\theta = 10.1$ °. The presence of this reflection indicates that the GO sheets stacked themselves on top of each other and became graphite-like during the simple drying procedure. PMMA showed the diffuse scattering typical of amorphous polymer. The 001 reflection appeared on the profiles of the nanocomposites with 5 and 10 % w/w GO loadings, overlapping with the scattering of PMMA. The excess amount of GO caused the strong interaction between the GO sheets themselves; as a result, the agglomeration was formed in the PMMA matrix. In contrast, for the nanocomposites with a low content of GO (up to 1 % w/w), the 001 reflection disappeared, which reveals the exfoliation and nano-dispersion of GO into the PMMA matrix. [23,24] Similar to the low content nanocomposites, as shown in the corner of the profiles, the 001 reflection of the GO interlayer was not observed for the dried co-aggregated precipitant of PMMA/GO with 1 % w/w GO loading, though it was detected for the physical mixture of

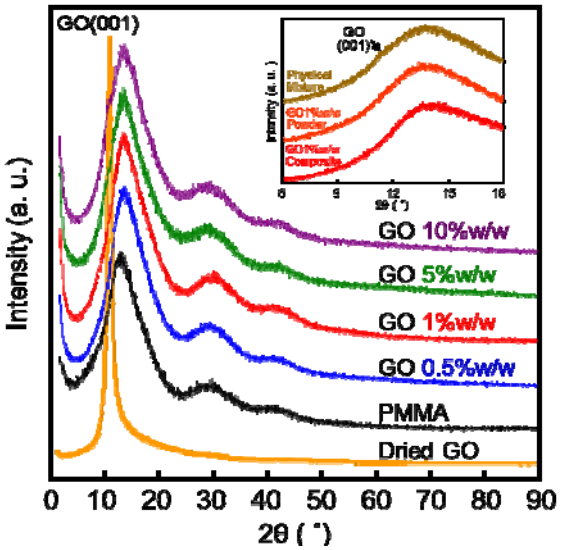

Figure 2. X-ray diffraction profiles of PVA film, PVA/GO nanocomposites and GO. The inserted figure on the upper right is the profiles of PVA/GO nanocomposite and physical mixture of PVA and GO 1 % w/w.

the PMMA powder and 1 % w/w of GO powder. This suggests that the mixing of PMMA and GO in the presence of water is necessary for the nano-dispersion of GO.

3.2 Mechanical properties

Figure 3(a) shows the stress (σ)-strain (ε) curves of the PMMA film and the PMMA/GO nanocomposites. The Young's modulus (E) of the nanocomposites dramatically increased when GO was incorporated. As for 1 % w/w GO loading, the E value (4.1 GPa) was double that of PMMA (2.2 GPa). This indicates that the GO sheets were exfoliated in the nanocomposites and the high aspect ratio of GO was effectively imparted with their rigid structure. Figure 3(b) shows the effect of GO loading on the E, tensile strength (σ_{max}), elongation at break (ε_{max}), and the toughness (K) of the PMMA film and the PMMA/GO nanocomposites. As shown in the figure, not only the E and σ_{max} value, but also K value increased up to 1 % w/w loading of GO. The increase in K value resulted from the maintaining of the ε_{max} value, which generally decreases drastically for nanocomposites reinforced using rigid filler. Typically, when stress is applied to the nanocomposite, the stress concentrates at the interface of the polymer matrix and rigid filler. The concentrated stress causes crazes and crack propagation, which results in the destruction of the entire composite. Therefore, the increase in the ε value or the K value has been rarely reported for the rigid filler composites previously. [25] In contrast, the ε value of the PMMA/GO nanocomposites remained almost the same as that of the PMMA film. As a result, the K value increased up to 35 % compared with that of the PMMA film. We can thus conclude that GO plays a role in the crack pinning of nanocomposites. Figure 3(c) and (d) shows the SEM photographs of the cross section of the PMMA and the PMMA/GO nanocomposites, respectively, after fracture.

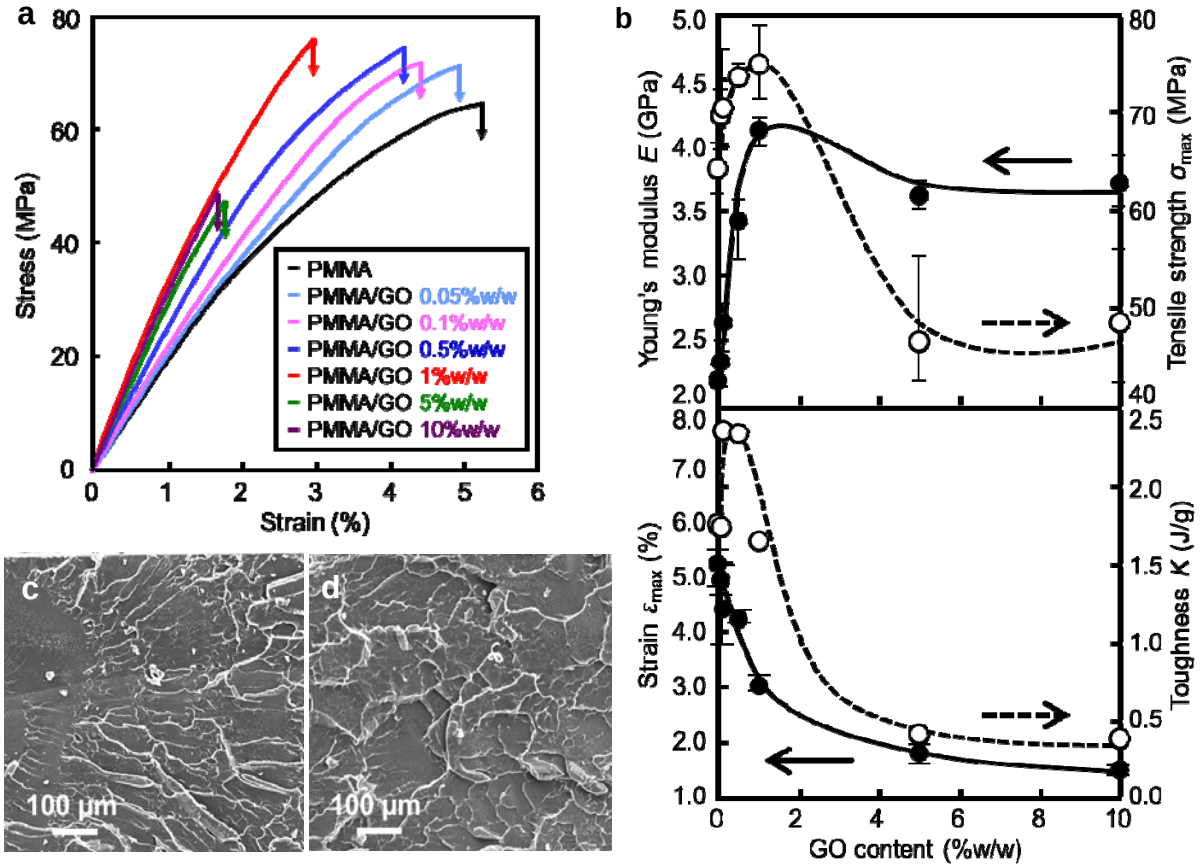

Figure 3. (a) Stress-strain curves of PMMA film and PMMA/GO nanocomposites; (b) Experimental Young's modulus (E), tensile strength (σ_{max}), strain (ε_{max}) and toughness (K) of the PVA/GO nanocomposites; SEM photographs of the cross section of (c) PMMA and(d) PMMA/GO nanocomposite (1 %w/w) after fracture.

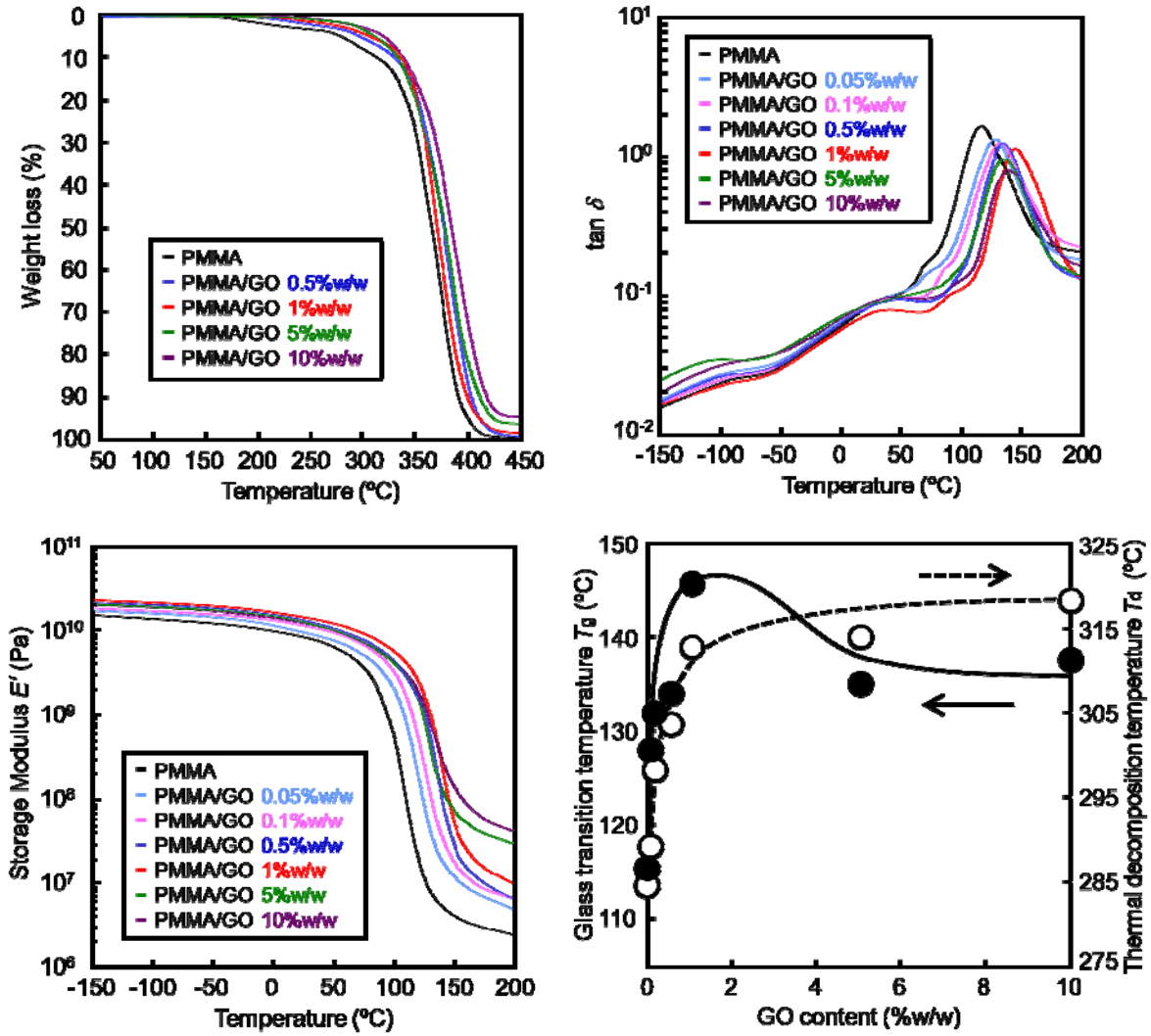

Figure 5. Temperature dependence of (a) storage modulus (E') and (b) tan δ of PMMA film and PMMA/GO nanocomposites. (c) Thermogravimetric traces of PMMA film and PMMA/GO nanocomposites; (d) Relationships between glass transition temperature (T_g), thermal degradation temperature (T_d) and GO content.

The PMMA had a conchoidal fracture, which is typical for amorphous glassy polymer, while the nanocomposite had a scaly pattern, which is completely different from the PMMA. This indicates that, in the nanocomposite, the GO was what prevented the crack propagation. These results show that our proposed fabrication process could successfully achieve the nano-dispersion of GO with a low content. When more GO was added to the polymer matrix (5, 10 % w/w), the ε value decreased drastically. As described above, in the nanocomposites with 5 and 10 % w/w GO loading, GO formed some graphite like structure. The interactions between the GO sheets, mainly by van der Waals force, stacked the sheets together and formed rigid GO agglomerates. These agglomerates reduced the aspect ratio of the filler and easily acted as crack initiations at the interface between the polymer matrix and the agglomerates. Therefore, the ε and σ values of the nanocomposites with GO loading of 5 and 10 % w/w decreased.

Figure 4(a) and (b) shows the temperature dependence of the storage modulus (E') and the mechanical tanδ of the PMMA film and the PMMA/GO nanocomposites, respectively. The main dispersion in tanδ, the so-called α_a, in the region from 100 ˚C to 150 ˚C is assigned as the glass transition temperature (T_g). It is apparent that the peak of the α_a dispersion largely

shifted to the higher temperature and the intensity decreased by the incorporation of GO. With only 1 % w/w GO loading, an increase of 40 ˚C was observed for the nanocomposites. The increase in T_g is attributed to the restriction of the mobility of the PMMA chains' interaction with the nano-dispersed GO sheets. This also appeared as the decrease in the *E'* value over the T_g was suppressed. Within the entire temperature range (−150 ˚C to 200 ˚C), the high *E´* value was maintained for the PMMA/GO nanocomposites. This indicates that GO functions as an excellent reinforcing filler.

3.4 Thermal properties

Figure 4(c) shows the TG traces of PMMA film and PMMA/GO nanocomposites. There was a definite enhancement in the thermal degradation temperature (T_d) by the incorporation of GO. Figure 4(d) shows the relationship between T_g, T_d and the GO content. The T_d of the nanocomposites increased linearly with the addition of GO up to 1 % w/w loading. A 28 ºC increase in T_d can be observed with only 1 % w/w of GO content This suggests that GO acts as a barrier to hinder the volatile decomposition products throughout the nanocomposites.

3.4 Barrier properties

Improvement in the barrier properties has often been reported for many kinds of polymer/clay nanocomposites. [26,27] Exfoliated clay with a high aspect ratio and effective surface area in the matrix widens the pathway for the permeating gas molecules. The strategy for improving the barrier properties can also be expected to work for the PMMA/GO nanocomposites because of the exfoliated morphology of the GO.

Figure 5 shows the O_2 gas permeability of the PMMA film and the PMMA/GO nanocomposites. Tsai *et. al.* reported a 50 % reduction of the gas permeability by the 5 % w/w incorporation of clay into PMMA. However, in this study it was obvious that the O_2 gas permeability was significantly suppressed with the addition of GO: the addition of only 1 % w/w of GO to the PMMA matrix decreased the permeability by 50 %. [28] Furthermore, the nanocomposite with 10 % w/w of GO was found to be almost completely impermeable. In the PMMA/GO nanocomposites, the nano-dispersion of GO with its high aspect ratio achieved the high performance in the barrier properties.

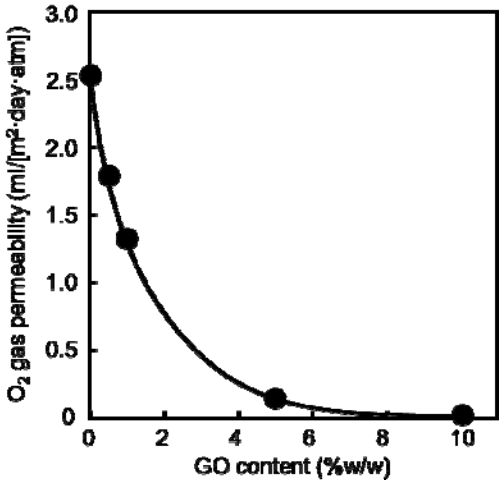

Figure 5. O_2 gas permeability of PMMA film and PMMA/GO nanocomposites.

4. Conclusion

We proposed an alternative to conventional procedures for fabricating PMMA/GO nanocomposites which using organic solutions and/or surfactants. We have developed an environmentally friendly technique in which PMMA is polymerized by soap-free emulsion polymerization and incorporated with GO by using an aqueous medium. The proposed method can be used to prepare nanocomposites with a wide range of GO content, rather than

the two extremes, low or high, it had been limited to before. This technique is practical for use in a wide variety of industries.

From the experimental results, GO was revealed to be highly exfoliated and nano-dispersed in the nanocomposites. In spite of the incorporation of rigid filler, the nanocomposites with a low content of GO maintained the ε_{max} value of the matrix. Therefore, not only the E and σ values but also the K value increased. The nanocomposites demonstrated high barrier properties, which depends on the high aspect ratio of GO. The nanocomposites with 10 % w/w GO loading were revealed to be almost completely impermeable. Furthermore, a remarkable enhancement in the T_g and T_d was observed by the incorporation of GO. Overall, not only excellent properties but also the unique morphology of GO was successfully imparted to the PMMA/GO nanocomposites.

References

[1] Lee C., Wei X., Kysar J. W., Hone J., *Science*, **321**, 385 (2008).
[2] Balandin A. A., Ghosh S., Bao W., Calizo I., Teweldebrhan D., Miao F., Lau C. N., *Nano Lett.*, **8**, 902 (2008).
[3] Iijima S., *Nature*, **354**, 56, (1991).
[4] Baughman R. H., Zakhidov A. A., Heer W. A., *Science*, **279**, 787 (2002).
[5] Morimune S., Kotera M., Nishino T., Goto K., Hata K., *Macromolecules*, **44**, 4415 (2011).
[6] Gong X., Liu J., Baskaran S., Voise R., Young J., James, S. *Chem. Mater*., **12**, 1049 (2000).
[7] Velasco C., Martinez A. L., Lozada M., Alvarez M., Castaño V. M., *Nanotechnology*, **13**, 495 (2002).
[8] Gojny H., Nastalczyk J., Roslaniec Z., Schulte K., *Chem. Phys. Lett*., **370**, 820 (2003).
[9] Moniruzzaman M., Winey K. I., *Macromolecules*, **39**, 5194 (2006).
[10] Trujillo M., Arnal M. L., Müller A. J., *Macromolecules*, **40**, 6268 (2007).
[11] Hirata M., Gotou T., Horiuchi S., Fujiwara M., Ohba M., *Carbon*, **42**, 2929 (2004).
[12] Morimune M., Nishino T., Goto T., *Polymer Journal* (2012).
[13] Kim H., Abdala A. A., Macosko W., *Macromolecules*, **43**, 6515 (2010).
[14] Bao Q., Zhang H., Yang J., Wang S. Tang D. Y., Jose R., Ramakrishna S. C., Lim T., Loh K. P., *Adv. Funct. Mater*., **20**, 782 (2010).
[15] Wang W. P., Pan C. Y., *Polym. Eng. Sci.*, **44**, 2335 (2004).
[16] Zhang H. B., Yan Q., Zheng W. G., He Z., Yu Z. Z., *ACS Appl. Mater. Interfaces*, **3**, 918 (2011).
[17] Hummers W. S., Offeman R. E., *J. Am. Chem. Soc.*, **80**, 1339-1339 (1958).
[18] Zhang Q., Naito K., Tanaka Y., Kagawa Y., *Macromolecules*, **41**, 536-538 (2008).
[19] Singh V. K., Patra M. K., Manoth M., Gowd G. S., Vadera S. R., Kumar N., *New Carbon Mater.*, **24**, 147-152 (2009).
[20] Yang, N., Zhai, J., Wan, M., Wang, D., Jiang, *Synthetic Metals*, **160**, 1617-1622 (2010).
[21] Kuznetsov, V. L. *Carbon*, **29**, 665-668 (1991).
[22] Ozawa, M., Inaguma, M., Takahashi, M., Kataoka, F., Krüger, A., Osawa, E. *Adv. Mater.*, **19**, 1201-1206 (2007).
[23] Liang J., Houng Y., Zhang L., Wang Y., Ma Y., Guo T., Chen Y., *Adv. Funct. Mater.*, **19**, 2297 (2009).
[24] Usuki A., Hasegawa N., Kadoura H., Okamoto T., *Nano Letters*, **1**, 271 (2001).
[25] Morimune S., Kotera M., Nishino T., *J. Adh. Soc. Jpn.*, **46**, 320 (2010).
[26] Russo G. M., Simon G. P., Incarnato L., *Nano Lett.*, **10**, 4970 (2010).
[27] Morgan A. P., Gamboa D., Holder K. M., Grunlan J. C., *Langmuir*, **27**, 12106 (2011).
[28] Tsai T.Y., JuLin M., Chang C. W., ChiLi C., *J. Phys. Chem. Solids*, **71**, 590 (2010).